Laboratory studies of H2SO4/H2O binary homogeneous nucleation from the SO2+OH reaction: evaluation of the experimental setup and preliminary results

L.-H. Young, D. R. Benson, F. R. Kameel, S.-H. Lee

HAL Id: hal-00304083
https://hal.science/hal-00304083

Submitted on 18 Jun 2008

**Atmospheric
Chemistry
and Physics
Discussions**

Laboratory studies of H$_2$SO$_4$/H$_2$O binary homogeneous nucleation from the SO$_2$+OH reaction: evaluation of the experimental setup and preliminary results

L.-H. Young[1,2], D. R. Benson[1], F. R. Kameel[1], and S.-H. Lee[1]

[1]Kent State University, Chemistry Department, Kent, OH 44240, USA
[2]China Medical University, Department of Occupational Safety and Health, Taichung, Taiwan

Correspondence to: S.-H. Lee (slee19@kent.edu)

Title Page

Abstract	Introduction
Conclusions	References
Tables	Figures

|◄ | ►|
◄ | ►

Back | Close

Full Screen / Esc

Printer-friendly Version

Interactive Discussion

Abstract

We have developed a new laboratory nucleation setup to study binary homogeneous nucleation (BHN) of sulphuric acid and water (H_2SO_4/H_2O). Here we provide a detailed evaluation of this new experimental setup and also discuss our preliminary results by comparing with other laboratory studies. H_2SO_4 is produced from the $SO_2+OH\rightarrow HSO_3$ reaction and OH radicals are produced from water vapor UV absorption. The residual H_2SO_4 concentrations ($[H_2SO_4]$) are measured at the end of the fast flow nucleation reactor with a chemical ionization mass spectrometer. The measured BHN rates (J) ranged from 0.02 and 550 $cm^{-3}\,s^{-1}$ at the residual $[H_2SO_4]$ from 10^8 to $10^{10}\,cm^{-3}$, a temperature of 288 K and relative humidity (RH) from 6 to 23%; J increased with increasing $[H_2SO_4]$ and RH. J also showed a power dependence on $[H_2SO_4]$ with the exponential power of 3 to 8. These results are consistent with other laboratory studies under similar $[H_2SO_4]$ and RH, but different from atmospheric field observations which showed that particle number concentrations are often linearly dependent on $[H_2SO_4]$. Both particle sizes and number concentrations increased with increasing $[H_2SO_4]$, RH, and nucleation time, consistent with the predictions from nucleation theories. Particle growth rates were estimated between 28 to 127 $nm\,h^{-1}$, much higher than those seen from atmospheric field observations, because of the higher $[H_2SO_4]$ used in our study. While these experimental results demonstrate a validation of our laboratory setup, there are also technical difficulties associated with nucleation studies, including wall loss and H_2SO_4 measurements.

1 Introduction

Atmospheric particles affect atmospheric composition, cloud formation, global radiation budget, and human health. Nucleation is a gas-to-particle conversion process in which new particles form directly from gas phase species (Seinfeld and Pandis, 1998) and is a key process that controls particle number concentrations. Field studies have

shown that new particle formation occurs ubiquitously in the atmosphere, ranging from ground-level rural and urban areas to the upper troposphere and lower stratosphere (Kulmala et al., 2004). The most common feature of the new particle formation events is a substantial increase of number concentrations of nucleation mode particles (di-
5 ameter <20 nm), reaching up to 10^5 to 10^6 cm^{-3} in the condensable vapor-laden air. The involvement of sulphuric acid (H_2SO_4) in nucleation has been widely suggested, with the binary (Vehkamäki et al., 2002; Yu, 2007), ternary (Korhonen et al., 1999; Napari et al., 2002), or ion-induced nucleation (Yu and Turco, 2000; Lee et al., 2003; Lovejoy et al., 2004). However, it was often found the nucleation rates predicted from
10 nucleation theories cannot explain the atmospheric observations and there are large discrepancies (e.g., Weber et al., 1996).

Table 1 summarizes the H_2SO_4/H_2O binary homogeneous nucleation (BHN) laboratory studies found in the current literature. Earlier laboratory studies typically produced H_2SO_4 vapors by vaporizing the liquid H_2SO_4 samples for simplicity and calculated the
15 saturation ratio, relative acidity, or the H_2SO_4 concentration ($[H_2SO_4]$) based on mass balance (Reiss et al., 1976; Mirabel and Clavelin, 1978; Wyslouzil et al.,1991; Viisanen et al.,1997). Other studies have produced H_2SO_4 from gas phase SO_2 by means of α-ray irradiation for ion-induced nucleation studies (Diamond et al., 1985; Mäkelä et al., 1995; Kim et al., 1997). In addition, Christensen et al. (1994) used photolytic excitation
20 of SO_2 (wavelength between 240 and 330 nm) in NH_3/H_2O ternary system to produce H_2SO_4.

A number of H_2SO_4/H_2O BHN studies were performed in continuous-flow reactor systems. For example, Wyslouzil et al. (1991) investigated the H_2SO_4, relative humidity (RH), and temperature dependence of nucleation rate (J). At relative humidity (RH)
25 between 0.6 to 65% and temperatures of 293, 298, and 303 K, they measured J between ~0.001 to ~300 cm^{-3} s^{-1} for calculated relative acidities between 0.04 and 0.46; the estimated numbers of H_2SO_4 molecules in the critical cluster ranged from 4 to 30. Viisanen et al. (1997) measured J between 2 to 3000 cm^{-3} s^{-1} for calculated $[H_2SO_4]$ between 1×10^{10} to 3×10^{10} molecules cm^{-3} at 298 K and ambient pressure; the esti-

Laboratory studies of H_2SO_4/H_2O binay homogeneous nucleation

L.-H. Young et al.

mated numbers of H_2SO_4 molecules in the critical cluster at 38% and 52% RH are 21 and 10, respectively. Ball et al. (1999) directly measured $[H_2SO_4]$ with a chemical ionization mass spectrometer (CIMS) and obtained J ranging from approximately 0.01 to 1000 cm^{-3} s^{-1} for $[H_2SO_4]$ between $\sim 2.5 \times 10^9$–1.2×10^{10} cm^{-3} at RH from 2–15%, 295 K and ambient pressure. The estimated numbers of H_2SO_4 and H_2O molecules in the critical clusters are between 7 to 13 and 4 to 6, respectively (Ball et al., 1999). With a similar approach with CIMS, Zhang et al. (2004) obtained J ranging from $\sim$0.3 to 500 cm^{-3} s^{-1} for $[H_2SO_4]$ from $\sim 4 \times 10^9$–1.0×10^{10} cm^{-3} at RH of $\sim$5%, 298 K and ambient pressure.

Reiss et al. (1976) and Boulaud et al. (1977) have noted the difficulties with the liquid H_2SO_4 samples; for example, the corrosiveness and extremely low vapor pressure of H_2SO_4, and the vapor equilibrium in the carrier gas and the homogeneity of the H_2SO_4/H_2O mixture are difficult to characterize. Boulaud et al. (1977) used in-situ gas phase reaction of $SO_3 + H_2O$ for the production of H_2SO_4 vapors, and obtained J of 1 cm^{-3} s^{-1} for $[H_2SO_4]$ from $\sim 10^{10}$–10^{11} cm^{-3} at RH from 15–70% and 293 K. Berndt et al. (2005, 2006) used the gas phase reaction of $SO_2 + OH$ to produce H_2SO_4 vapor, via the following reactions:

$$SO_2 + OH \rightarrow HSO_3 \qquad \text{(Rate limiting step)} \tag{R1}$$

$$HSO_3 + O_2 \rightarrow SO_3 + HO_2 \tag{R2}$$

$$SO_3 + 2H_2O \rightarrow H_2SO_4 + H_2O \tag{R3}$$
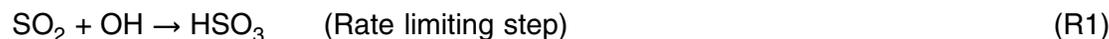
Berndt et al. (2005, 2006) then calculated $[H_2SO_4]$ from the estimated $[OH]$ and $[SO_2]$; $[OH]$ was calculated from titration reactions of hydrocarbons and OH. From this method, they obtained a low threshold for nucleation, $[H_2SO_4]$ of $\sim 10^7$ cm^{-3}, considerably lower than those from other previous laboratory nucleation studies (Viisanen et al., 1997; Ball et al., 1999; Zhang et al., 2004). Recently, Berndt et al. (2007) have also suggested a new pathway to produce particles from SO_2 and OH other than through

Laboratory studies of H_2SO_4/H_2O binay homogeneous nucleation

L.-H. Young et al.

Reactions (R1–R3), in which gas phase HSO_5 may be produced to contribute to new particle formation.

We have performed laboratory studies of H_2SO_4/H_2O binary homogeneous nucleation in a fast flow reactor at 288 K, RH from 5 to 25%, and the ambient pressure. Our laboratory system is constructed based on the selective combination of the experimental methods utilized in Berndt et al. (2005, 2006), Ball et al. (1999) and Zhang et al. (2004). Similarly to Berndt et al. (2005, 2006), we also used (R1–R3) to in-situ produce H_2SO_4; but we measure H_2SO_4 directly with a CIMS, the same method utilized as in Ball et al. (1999) and Zhang et al. (2004). Unlike Berndt et al. (2005, 2006) where OH forms from ozone UV reactions, in the present study OH is produced by water photolysis to allow direct measurement of [OH]. The primary objective of this study is to evaluate the performance of the nucleation experimental setup from the measured nucleation rates at various [H_2SO_4] and RH conditions.

2 Experimental setup

Our nucleation experimental setup consists of (a) an OH generator, (b) a temperature- and RH-controlled, fast flow nucleation reactor, (c) a high sensitivity, atmospheric pressure CIMS to measure low concentrations of H_2SO_4, and (d) TSI aerosol spectrometers to measure aerosol sizes and concentrations (Fig. 1). Table 2 shows the typical experimental conditions used in the present study.

2.1 OH radical and sulphuric acid generation

H_2SO_4 vapor is produced in-situ via (R1–R3). SO_2 is taken from standard SO_2 gases (1, 2.5, and 100 ppm) that are further diluted with standard air. OH forms from the photo-dissociation of H_2O vapor in a quartz tube (13 cm long with 2.54 cm I.D.), using a mercury lamp (Pen-Ray 11SC-1) filtered for $\lambda < 185$ nm with a bandpass filter (Omega Optical XB32 185NB20). Both the lamp and the filter are housed inside a temperature-

Title Page

Abstract	Introduction
Conclusions	References
Tables	Figures

|◄ | ►|

◄ | ►

Back | Close

Full Screen / Esc

Printer-friendly Version

Interactive Discussion

controlled metal box, which is purged with a constant N_2 flow rate to provide a stable photon flux. At the bottom of the box, there is a radiation exit slit with the long side parallel to the flow direction. The photon flux exiting the light source is detected as a function of distance using a solar-blind CsI phototube (Hamamatsu R5764), which is calibrated against a NIST-certified Si photodiode (40599S). The photocurrents are measured with a pico-ampere meter (Keithley 6517A) or converted to voltage signals with resistors and measured by a voltage meter (Fig. 2a). By measuring H_2O mixing ratios and UV photon intensities, [OH] is calculated based on the known photochemical reaction rates (absolute calibration) (Cantrell et al., 1997). For example, the photon flux, I, at radiation wavelength, λ (nm), is determined by:

$$I(\lambda) = \frac{A(\lambda)}{e \times \varepsilon(\lambda)} \tag{1}$$

where A is the measured ampere at λ, e is the electronic charge (1.6×10^{-19} C), and ε is the quantum efficiency of the NIST-certified photodiode at λ. [OH] then is calculated from the following equations (Cantrell et al., 1997):

$$[OH] = J_{H_2O}[H_2O]t_p \tag{2}$$

$$J_{H_2O} = I\sigma\phi \tag{3}$$

where J_{H_2O} is the H_2O photolysis rate, σ the absorption cross-section of water vapor ($\sigma=7.14 \times 10^{-20}$ cm^2 molecule^{-1} (Cantrell et al., 1997), ϕ the quantum yield [ϕ(OH)= 1.0 (DeMore et al., 1997)], and t_p the photolysis time. [H_2O] is determined from the measured temperature and RH (%):

$$[H_2O] = \frac{RH}{100}\frac{p_s}{p_t}N_d \tag{4}$$

where p_s is the H_2O saturation vapor pressure [e.g., 1612 Pa (or 12.09 torr) at 288 K (NIST, 2005)], p_t the total pressure, and N_d the number concentration

Laboratory studies of H_2SO_4/H_2O binay homogeneous nucleation

L.-H. Young et al.

of dry air molecules. At typical experimental conditions, A=1.2×10^{-5} A cm^{-2}, I=1.4×10^{14} photon cm^{-2} s^{-1}, and hence typically J_{H_2O}=9.7×10^{-6} s^{-1}. Thus the [OH] produced were at the 10^9–10^{10} cm^{-3} range as a function of RH and t_p (Fig. 2b). When [SO$_2$]≫[OH], the initial [H$_2$SO$_4$]=[OH] based on Reaction (R1).

2.2 Nucleation reactor

The nucleation reactor is made of a fast-flow reactor (Pyrex cylinders with a length of 50, 88, or 100 cm and with an inner diameter of 2.54 or 5.08 cm) with a laminar, fast flow. The reactor is also controlled for temperature with a refrigerating/heating circulating bath (Cole-Parmer Model 12101-31) and washed with distilled water daily to remove H$_2$SO$_4$ and particles deposited on its inside wall during the previous day's experiments. The total pressure in the nucleation reactor is ~97.3 kPa (slightly higher than the room air pressure to prevent leak from the room air), 288 K, and the RH of ~5–25%. The total flow rate is up to 1.7–5.3 l min^{-1} and t_n was estimated to be from 5–59 s, when assuming that nucleation occurs in the entire nucleation reactor. We believe that this time scale is sufficient for converting SO$_2$ to H$_2$SO$_4$ and also for particle nucleation and yet, short enough to minimize the wall loss of H$_2$SO$_4$ and particles. The measured aerosol sizes and number concentrations increased with increasing t_n (in the range from 4–57 s), indicating that nucleation dominates over condensation processes and in this condition, t_n can be assumed to be the same as the residence time in the nucleation reactor.

Because of the wall loss and condensation of H$_2$SO$_4$, the CIMS-measured [H$_2$SO$_4$] is not the initial [H$_2$SO$_4$] and is rather the equilibrium or residual [H$_2$SO$_4$]. This is the same situation as with other nucleation studies that used CIMS (Ball et al., 1999; Zhang et al., 2004). In the present study, we provide the CIMS-measured, residual [H$_2$SO$_4$] to compare with these other studies using CIMS, but we also provide wall loss factors (WLFs) (the ratios of the initial [H$_2$SO$_4$] over the residual [H$_2$SO$_4$] at the end of the nucleation reactor) and the initial [H$_2$SO$_4$] (which are the same as the produced [OH],

because $[SO_2]'' [OH])$ (Fig. 2b). WLFs of H_2SO_4 were estimated by assuming that wall loss is a diffusion-limited process based on Hanson and Eisele (2000) and Benson et al. (2008). Figure 3 shows the calculated the WLFs as a function of t_n and RH for different nucleation tubes used in this study (I.D.=5.08 cm and 2.54 cm). At the typical experimental conditions used in this study, the estimated wall loss factors ranged from 2 to 12 for the t_n from 20 to 54 s and RH from 5 to 25% for the nucleation reactor with I.D. 5.08 cm (Fig. 3a).

2.3 Particle measurements

A nanoparticle differential mobility analyzer (Nano-DMA) (TSI 3080N) and an ultrafine water condensation particle counter (CPC) (TSI 3786) are used for particle number and size distribution measurements. These aerosol instruments were operated in two modes, the CPC standalone mode and the Nano-DMA/CPC combination mode. In the standalone mode, CPC has a 50% detection efficiency at ~2.5 nm and gives total particle number concentrations every 5 s. The CPC inlet flow is set at 0.6 liter per min (lpm). In the Nano-DMA/CPC combination mode, size-resolved particle number concentrations are obtained from 2.5–102 nm every 180 s. The SMPS inlet and sheath flows are set at 0.6 and 6 lpm, respectively.

The integrated "total" particle number concentrations from the combination mode were on average five to ten times lower than the total particle number concentrations from the standalone mode. This concentration difference is in part because of the additional tubing length involved in the SMPS/CPC measurement in this study. Based on Baron and Willeke (2001), the estimated fractional penetration efficiency of 3 nm particles through the additional 39-cm long cylindrical tubing at 0.6 lpm is 0.65. In addition, it is possible that the CPC may be able to detect H_2SO_4 particles smaller than the stated minimum measurable size (~2.5 nm). When the CPC is operated with the nano-SMPS, some of the particles smaller than 2.5 nm may be excluded in the nano-DMA, hence further contributing to the concentration difference. Note that however Berndt et al. (2006) showed reasonable agreement between the combination and standalone

mode as opposed to the findings in the present study.

The J were determined by the measured particle number concentrations (N) and t_n. In most cases the N were determined using the CPC standalone mode, except when the size distribution measurements were involved. Because critical clusters ($\sim$1 nm) are typically smaller than the minimum measurable size of the CPC, the J reported here, strictly speaking, is not the actual nucleation rate, but rather the formation rate of particles with diameters larger than $\sim$2.5 nm, the so-called "apparent formation rate" (Kerminen and Kulmala, 2002). However, when condensation and coagulation growth are negligible which was the case for most of our experiments, the values estimated from such a calculation are close to the actual J values (Kulmala et al., 2004).

The numbers of H_2SO_4 molecules (n) in the critical clusters are calculated with the J vs. [H_2SO_4] at specific values of RH and absolute temperature T, based on the first nucleation theorem (Kashchiev, 1982; Strey and Viisanen, 1993):

$$\left. \frac{\partial \ln J}{\partial \ln[a_1]} \right|_{a_2, T} \approx n \qquad (5)$$

where a_1 and a_2 are the activity of species 1 and 2, respectively. In practice, the n values for H_2SO_4 molecules can be approximated by fitting the data points with power regression:

$$J = c[H_2SO_4]^n \qquad (6)$$

where c is a constant, at specific values of temperature and RH.

2.4 H_2SO_4-CIMS

Our CIMS was built by Greg Huey's group at Georgia Tech based on (Eisele and Tanner, 1993). The CIMS instrument is constructed from an ion source, an ion molecular reactor, and a quadrupole mass spectrometer. The following ion molecule reaction

$$NO_3^- + H_2SO_4 \rightarrow HNO_3 + HSO_4^- \qquad (R4)$$

is used to detect H_2SO_4 (Viggiano et al., 1997). This reaction scheme has been proven to be very effective for H_2SO_4 measurements, and this is one of the very few methods currently available to detect H_2SO_4 at atmospheric concentrations. This low detection limit is achieved because of its high reaction rate, high selectivity against other species, and the atmospheric pressure ionization used.

The $^{210}P_o$ radiation source is used as an ion source. The ion source region also has a unique design to prevent artifact H_2SO_4 detection. Because OH radicals also form from water molecule dissociation reactions in the ion source region ($^{210}P_o$ radiation), there is a possibility that those OH radicals react immediately with the SO_2 in the air samples to produce H_2SO_4. To eliminate such artifacts of H_2SO_4 formation, a weak electric field is applied between the ion source region and the center of the sampling inlet so that only the electrically charged NO_3^- ions (not the neutral OH radicals) travel through to the center of the sampling inlet to react with H_2SO_4. In addition, C_3F_6 gases are also mixed with HNO_3 gases so that OH radicals are efficiently removed by C_3F_6. With the current CIMS configuration, the background $[H_2SO_4]$ is negligible even when high concentrations of SO_2 gases are introduced into the CIMS. A collision dissociation chamber (CDC) is applied to dissociate the weakly bonded ion molecule clusters of sulphuric acid, nitric acid, and water molecules by low energy collisions with N_2 molecules to provide simpler ion peaks. Ions are focused by an octopole before reaching the quadrupole mass filter (Extrel) and then detected by a channeltron detector (K+M). The pressures in the CDC, octopole, and quadrupole are about 10^1, 10^{-1}, and 10^{-3} Pa, respectively.

$[H_2SO_4]$ are calculated from the ratio of the HSO_4^- to NO_3^- ion counts $[HSO_4^-]/[NO_3^-]$, the rate constant k of (R1), and the reaction time t_r based on Huey (2007):

$$[H_2SO_4] \approx \frac{[HSO_4^-]}{[NO_3^-]kt_r} \tag{7}$$

Where k for (R1) is 1×10^{-9} cm^3 molecule^{-1} s^{-1} (Viggiano et al., 1997) and t_r is typically 0.05 s under the present experimental setup. $[NO_3^-]$ (that is, $[N^{16}O_3^-]$) is obtained indi-

rectly by measuring its isotope [$N^{18}O_3^-$] and by taking the natural isotopic ratio of ^{16}O and ^{18}O abundances (99.8%:0.2%) into account. Although [$N^{18}O_3^-$] varied from day to day, the resulting [HSO_4^-]/[NO_3^-] ratio is fairly constant for a given [H_2SO_4]. Before each experimental run, the CIMS is adjusted to obtain [$N^{18}O_3^-$] between 1500 to 3500 Hz.

⁵ Thus [NO_3^-] are from 8×10^5 to 2×10^6 cm^{-3} and in this condition, 1 Hz of HSO_4^- ion count corresponds to [H_2SO_4] from 1×10^4 to 3×10^4 cm^{-4}. Since the instrument noise of [HSO_4^-] is ~20 Hz, the CIMS detection limit for H_2SO_4 is from 2×10^5 to 6×10^5 cm^{-4}.

2.5 Flow rate, RH and temperature measurements

The total flow rate (Q_{total}) typically ranged from 1.7 to 5.3 lpm and composed primarily of
¹⁰ SO_2 and N_2. The SO_2 flow rate (Q_{SO_2}) varied between 0.01 to 2 lpm, depending on the SO_2 concentration of the cylinder. The dry N_2 flow rate was adjusted simultaneously with the Q_{SO_2} to maintain a constant total flow. The H_2O flow (i.e., humidified N_2 flow) varied between 0.01 to 0.2 lpm to maintain the target RH values. The O_2 flow was maintained at 0.001 lpm regardless of the total flow rate.

¹⁵ The photolysis tube was exposed to indoor temperature (295±2 K), and the nucle-ation tube was maintained at 288±0.05 K with a refrigerating circulating bath (Cole-Parmer Model 12101-31). RH is controlled mainly by changing the flow rates of wa-ter vapor into the nucleation reactor. There are three sets of temperature, RH, and pressure sensors in our nucleation reactor, temperature/humidity sensors (Campbell
²⁰ Scientific CS215) and pressure gauges (Granville-Phillips 275).

Only high purity standard gases (nitrogen, oxygen, SO_2 and NH_3) (Linde Gas and Airgas Inc.) and distilled water are introduced in the nucleation region. We have used the silicon phosphates ammonia scrubber (Perma Pure Inc.) to test the effects of possi-ble ammonia impurities in our system on the H_2SO_4–H_2O BHN experiments, and those
²⁵ effects were found negligible. Test results with CO scrubbers (Carus Carulite 300) also showed that CO impurities in the photolysis and nucleation reactor are negligible. The

flows of these gases in the water photolysis cell, the nucleation reactor, and CIMS are controlled with seven high precision mass flow controllers (MKS). These mass flow controllers were also regularly calibrated with a standard flow meter (DryCal DC-2, Bio International Corp.).

⁵ ## 3 Experiment results

3.1 SO_2, OH, H_2O and O_2 effects on H_2SO_4 and particle production

In order to confirm that nucleation takes place via (R1–R3) as designed, we first examined the effects of precursor gases by observing the changes in the production of H_2SO_4 and new particles after adding or removing the gas phase species in question.
¹⁰ Figure 4 shows how H_2SO_4 and particle concentrations are affected by SO_2 and OH at RH of 15% and t_n of 19 s. The production of OH was controlled by switching the UV radiation on or off in the presence of H_2O vapor. Figure 4a shows the experiment sequence, (1) adding OH, (2) adding OH and SO_2 together, (3) removing OH only, and (4) removing both SO_2 and OH from the flow reactor, in the presence of H_2O vapor
¹⁵ and O_2. This sequence was repeated for three runs with different Q_{SO_2} of 0.6, 0.45, to 0.4 lpm. The respective initial SO_2 concentrations [SO_2], calculated based on the SO_2 source concentration and the ratio of the Q_{SO_2} to the Q_{total}, were 0.12, 0.09, and 0.08 ppm. Figure 4b shows the distinctive rise or drop of [H_2SO_4] when switching the Q_{SO_2} on or off and these results confirm that H_2SO_4 vapor has formed from (R1–R3)
²⁰ and new particles formed via nucleation involving H_2SO_4 vapor.

Figure 4b also shows that there was no production of H_2SO_4 and new particles unless SO_2 was added to OH, O_2, and H_2O (steps (1) and (2)). It was consistent throughout our experiments that the background values of [H_2SO_4] and N were negligible in the absence of SO_2, indicating that the experimental setup was well constructed and
²⁵ the flow reactor is fairly clean. However, at step (3) in the absence of OH and in the presence of SO_2, both the [H_2SO_4] and N dropped sharply to a lower level, but above

the initial background values (without SO_2). This result was not expected from (R1–R3). In addition, since we have used much higher [SO_2] than [OH] (at least three orders of magnitude higher), [H_2SO_4] should be the same as [OH] and independent of [SO_2] and thus N would also be constant at the same t_n and RH. However, from the first sequence run to the third one, the gradual decrease of [H_2SO_4] from 1.6×10^8 to $1.5 \times 10^8 \, cm^{-3}$ and N from 48 to $30 \, cm^{-3}$ was a result of the reduced amount of SO_2 added to the system (Fig. 4b). Figure 5a shows more distinctive dependence of [H_2SO_4] and N on [SO_2] at constant RH and t_n. Similar dependence of N and [H_2SO_4] on [SO_2] can be seen from other figures presented here (Figs. 6–12). This [H_2SO_4] dependence on [SO_2], together with [H_2SO_4] and new particle production in the absence of OH, suggest a possible incomplete mixing between SO_2 and OH or/and an unknown process of the H_2SO_4 and new particle production, as will be discussed in Sect. 4.6.

With similar experiment sequences, we tested the effects of H_2O on the production of H_2SO_4 and particles. As expected, removing H_2O reduced the production of both H_2SO_4 and new particles. For example, with the presence of H_2O, [H_2SO_4] and N were $1.6 \times 10^8 \, cm^{-3}$ and $9 \, cm^{-3}$, respectively, at RH=15%, whereas with the removal of H_2O, [H_2SO_4] and N were $7.2 \times 10^6 \, cm^{-3}$ and $4 \, cm^{-3}$, respectively (not shown). It is noted that, due to the experimental setup, the removal of H_2O vapor did not make the system completely free of H_2O and the minimum RH attained in the current system was 4%.

In contrast to the cases of SO_2, OH and water, the removal of O_2 from the system had only minor effects on the production of H_2SO_4 and new particles. With or without O_2, the [H_2SO_4] and N were nearly the same. In addition, both the [H_2SO_4] and N became more fluctuating without O_2. The lack of O_2 effects was not expected because SO_3 would not form without O_2, according to Reaction (R2). We believe there was no leak into the system from the room air, because the pressure of the flow reactor was always maintained above the ambient pressure. Some O_2 may have come from the gas cylinders as a part of the impurities.

Lower concentrations of SO_2 were used by diluting standard SO_2 gases (1, 2.5, and

Laboratory studies of H_2SO_4/H_2O binay homogeneous nucleation

L.-H. Young et al.

100 ppm), to obtain a given J value. We also have seen that a substantially higher initial [SO_2] was required when diluting the SO_2 from the 100 ppm cylinder than from the 1 ppm cylinder (Fig. 5). Figure 5 shows the measured [H_2SO_4] and N at RH of 15%, Q_{total} of 5 lpm and t_n of 19 s. For example, it required an initial [SO_2] of 3.2 ppm

5 for the 100-ppm experiment to obtain J of 0.8 cm^{-3} s^{-1}, while only 0.08 ppm SO_2 was required for the 1-ppm experiment to form similar numbers of new particles. The flow ratios of Q_{SO_2} to Q_{total} were from 0.03–0.15 and from 0.025–0.04 for the 1 ppm and 100 ppm SO_2 cylinder experiments, respectively. Because SO_2 molecules were released near the centerline of the flow reactor, it would take a longer time for SO_2

10 molecules to be vigorously mixed with OH radicals at lower mixing ratios than at higher mixing ratios. This will lead to a reduced production efficiency of H_2SO_4, hence lower particle production. If the data for the 100 ppm experiment were extrapolated to [SO_2] of 0.03 ppm, the expected [H_2SO_4] would be 8.1×10^7 cm^{-3}, which is in fact about a factor of two lower than the measured [H_2SO_4] (1.4×10^8 cm^{-3}) from the 1 ppm experiment

15 with the same [SO_2]. The extrapolated results clearly suggest the H_2SO_4 production efficiency of 100 ppm experiments is lower than the 1 ppm experiments. However, this "non-overlapping" data may suggest something more complex than we currently understand.

3.2   Nucleation time (t_n) dependence of particle numbers (N) and [H_2SO_4]

20 Figure 6 shows the effects of t_n on the production of H_2SO_4 and N. t_n was varied between 4 and 9 s, by using two nucleation tubes with similar lengths (L of 80 cm and 82 cm) but different diameters (I.D.=2.54 cm and 5.08 cm) at Q_{total} of 5 lpm and RH of 15%. The initial [SO_2] varied from 0.03 to 0.15 ppm in the two experiments and were identical for these two different t_n at the constant Q_{total}. As t_n increased from 4 to 19 s ,

25 N increased while [H_2SO_4] decreased. The positive correlation between the N and t_n suggests that the nucleation process, rather than the condensation process, dominates within the t_n from 4 to 19 s. Therefore, again it is reasonable to assume t_n values are

the same as the flow residence times in such a condition. Note that the calculated J from the experiments with t_n of 4 s and 19 s were on the same order of magnitude (0.3–2.1 cm^{-3} s^{-1} vs. 0.3–2.7 cm^{-3} s^{-1}), but the CIMS-measured [H$_2$SO$_4$] were different. In fact, [H$_2$SO$_4$] at t_n of 4 s was about a factor of two higher than that at t_n of 19 s (1.2–2.1×10^8 cm^{-3} vs. 3.2–5.8×10^8 cm^{-3}). Since the J values were comparable, it is likely that the [H$_2$SO$_4$] difference was mostly due to the increased wall loss at longer t_n. These results also highlight a technical issue when comparing [H$_2$SO$_4$] with different t_n.

Figure 7 also shows the similar wall loss effects on the residual [H$_2$SO$_4$]. At Q_{total} of 4.1, 2.6, and 1.8 lpm (the corresponding t_n were 24, 37, and 54 s, respectively) and Q_{SO_2} varied between 0.03 and 0.15 lpm and with similar initial [SO$_2$] (i.e., 4.9, 4.6, and 4.4 ppm), the CIMS-measured [H$_2$SO$_4$] decreased from 2.5×10^9 to 1×10^8 cm^{-3} with increasing t_n.

3.3 Number concentrations (N) vs. particle sizes (D_p)

We also investigated how N varies with D_p and how N and D_p vary as a function of t_n and the initial [SO$_2$] at constant RH (e.g., 23%) (Figs. 8 and 9). In this series of experiments, Q_{total} was decreased to increase t_n and the initial [SO$_2$]. At RH of 23% and t_n of 24 s, when the initial [SO$_2$] was raised from 2.9 to 4.9 ppm, N increased from 220 to 6.9×10^3 cm^{-3} and D_p increased from 3.6 to 5.0 nm (Fig. 8a). The corresponding [H$_2$SO$_4$] ranged from 1.5×10^9 to 2.4×10^9 cm^{-3}. Such increases of N and D_p with increasing initial [SO$_2$] were even more substantial at the t_n of 54 s; the N increased from 1.4×10^4 to 5.5×10^5 cm^{-3} and the D_p increased from 5.6 to 8.2 nm when the initial [SO$_2$] increased from 4.4 to 11.1 ppm (Fig. 8c). As t_n increased from 24 to 54 s, with similar initial [SO$_2$] (4.9, 4.6, and 4.4 ppm), N also increased from 6.9×10^3 to 1.4×10^4 cm^{-3} and the D_p increased from 5.0 to 5.7 nm (Fig. 9). These results indicate larger N and D_p at higher t_n, consistent with the predictions from nucleation theories. However, these results also show that the measured N in these nucleation experiments is also

related to D_p, which brings additional complexity to the interpretation of J from the measured N and t_n.

3.4 The RH effects on nucleation rate (J) and particle size (D_p)

Figure 10 shows the RH effects on the production of H_2SO_4 and particles at constant t_n
(e.g., 19 s). Q_{total} (5 lpm) and the nucleation reactor's I.D. (5.08 cm) and L (82 cm) were identical for these three RH levels. The initial $[SO_2]$ was between 2.4 and 4 ppm for RH of 11 and 15%, while the initial $[SO_2]$ was between 0.2 and 1 ppm for RH of 23%. At $[SO_2]$ of 2.4 ppm, for example, $[H_2SO_4]$ and J doubled from 6.5×10^8 to 1.6×10^9 cm^{-3} and 1 to 2 cm^{-3} s^{-1}, respectively, when the RH was raised from 11 to 15%, showing higher productions of H_2SO_4 and N at higher RH.

Figure 11 shows the particle size distributions measured at Q_{SO_2} of 0.1 lpm, Q_{total} of 2.6 lpm, the initial $[SO_2]$ of 3.8 ppm, and t_n of 38 s for RH of 22%, 26%, and 30%. As RH increased from 22 to 30%, the CIMS-measured $[H_2SO_4]$ increased from 7.3×10^8 to 1.0×10^9 cm^{-3} and N increased from 5.9×10^3 to 1.1×10^5 cm^{-3}. The calculated J were 160, 810, 3010 cm^{-3} s^{-1} at 22%, 26%, and 30% RH, respectively. The mode diameter also increased from 5.1 to 6.4 nm with increasing RH due to the increased H_2SO_4 production and particle growth. These results are consistent with the predictions of nucleation theories, higher H_2SO_4 production, higher nucleation rates and larger particle sizes at higher RH.

3.5 The $^{34}SO_2$ experiments

The SO_2 + OH experiments were also carried out with 2.5 ppm isotope $^{34}SO_2$ gases, instead of $^{32}SO_2$ gases, to test the validity of our nucleation experiments (Fig. 12). These isotope experiments were made at RH of 15%, temperature of 288 K, t_n of 10 s and the initial $[SO_2]$ ranging from 0.15–0.9 ppm. When the $^{34}SO_2$ gases were introduced into the system, both $H^{34}SO_4^-$ and $H^{32}SO_4^-$ ion peaks appeared and they

were positively correlated with the $^{34}SO_2$ flow rates, consistent with the $^{32}SO_2$ results (e.g., Fig. 11). The $H_2^{32}SO_4$ in Fig. 12a was resulted from the impurity of $^{32}SO_2$ in the $^{34}SO_2$ gas cylinder.

4 Discussions

4.1 Uncertainties in the particle measurement

The measured particle concentrations were generally not as stable and reproducible as the H_2SO_4 measurements. Overall, the relative standard deviation for the $[H_2SO_4]$ is only 0.06 and for the N is 0.39 during a 23-min period of the experiments, for example. Most of the present data however were taken over a much shorter period (<3 min). The reproducibility of the particle and H_2SO_4 measurements can be examined when the same experimental condition is repeated several times. For example, the percentage differences between two measurements with the same $[SO_2]$ were less than 6% for the $[H_2SO_4]$ and between 8–10% for the N (Fig. 10c). In addition, as described in Sect. 2.3, there are differences of a factor of five to ten between the N values measured by the CPC standalone mode and by the SMPS/CPC combination mode.

4.2 H_2SO_4 wall loss and its effects on the CIMS-measured $[H_2SO_4]$

Figure 13 shows hypothetical processes that are involved in H_2SO_4 loss in the nucleation reactor, including loss to the wall, by nucleation and condensation. There are substantial wall losses of H_2SO_4 inside the flow reactor and as shown by the lower $[H_2SO_4]$ at longer t_n (Figs. 6 and 7). The wall loss is a limitation of flow tube experiments, especially when the nucleation reactors have small inner diameter. In addition, other processes which can enhance or reduce the H_2SO_4 losses will also change the penetration efficiency of H_2SO_4 as discussed below.

Firstly, the H_2SO_4 wall loss depends on the flow rate, tube length, and diffusion coefficient. As shown in Figs. 6 and 7, we observed an anti-correlation between $[H_2SO_4]$ and t_n. This observation is consistent with Hanson and Eisele (2000) which showed that wall loss of H_2SO_4 in a fast flow reactor can be expressed with a first order rate

5　and nucleation time (as illustrated in Fig. 3). This trend can also be attributed to the higher particle concentration and hence more H_2SO_4 loss via nucleation as well as condensation, especially at longer t_n. The second factor is less important when the J is small.

　　Secondly, in the present experimental setup, H_2O molecules participate in both the

10　H_2SO_4 formation and aerosol nucleation process. This is because increasing $[H_2O]$ would increase the [OH] and thus H_2SO_4 production (R1), and also favor the hydration of H_2SO_4 molecules. The addition of H_2O molecules to H_2SO_4 molecules can also reduce the diffusion coefficients and thus decrease the wall loss. For example, Hanson and Eisele (2000) found a $\sim$20% reduction in effective diffusion coefficients of H_2SO_4

15　as RH increased from 0 to 40%. Such RH effects are also shown on the estimated WLFs (Fig. 3). The overall RH effect is an increase of the particle production and the penetration efficiency of H_2SO_4 molecules at higher RH.

　　From the above qualitative assessments of the wall loss of H_2SO_4, there are several factors that can affect the CIMS-measured, residual $[H_2SO_4]$, including RH, t_n, and the

20　diameter of the nucleation reactor. Most of these factors are dependent on the experimental setup, such as the physical dimensions and flow characteristics. Therefore, comparisons of the $[H_2SO_4]$ measured by CIMS and nucleation rates from different studies require a caution.

4.3　Nucleation rate (J) calculations

25　There are several factors that should be taken into account for nucleation rate calculations, including particle sizes, t_n, $[H_2SO_4]$ and RH. In nucleation experiments, particle nucleation rates are calculated from the measured N and t_n. The calculated J values shown here, as well as in other laboratory studies such as Ball et al. (1999), Zhang et

al. (2004) and Berndt et al. (2005, 2006), are the production rates of particles larger than 3 nm, and thus again the "apparent" formation rates. Several competing processes simultaneously take place in the nucleation reactor, such as nucleation, wall loss, and coagulation and condensation growth (Fig. 13). These processes, however,
also affect the measured $[H_2SO_4]$, N, and D_p, and in turn, affect the calculated J and the J dependence on $[H_2SO_4]$ (Fig. 14).

Our results show that the measured particles are not at the same size and both the N and D_p vary as a function of $[H_2SO_4]$, RH and t_n (Figs. 8, 9, 11). Also, at high t_n, the condensation growth and wall loss of H_2SO_4 becomes more important. At higher J
values, N can be even anti-correlated with $[H_2SO_4]$ (Benson et al., 2008), because condensation growth becomes to dominate over nucleation processes with larger particle surface areas (at higher N and D_p). If coagulation process is comparable to that of the nucleation process, it will lead to the reduced N and subsequently underestimated J (Wyslouzil et al., 1991). In addition, this kind of error increases with increasing particle
number concentration (or J values). Under such a circumstance, the underestimated J at the high end of the concentration range will in turn reduce the steepness of the slope of the power relationship between J and $[H_2SO_4]$. On the other hand, enhanced condensation growth will allow more particles to grow larger than 3 nm, leading to an increase of N and subsequently an overestimated J (Kulmala et al., 2006). Ball et
al. (1999) have noted that the predicted J values are larger than the observed J values at the low and high-end of the $[H_2SO_4]$ range when using a single power regression.

To obtain accurate "apparent" formation rates (which are referred as to J in this study), nucleation experiments must be conducted below the level at which nucleation dominates over coagulation or condensation growth process (for example, at lower
H_2SO_4 concentrations, lower particle number concentrations and shorter t_n). The effect of condensation growth is unavoidable, however, because H_2SO_4 condensation is needed for nucleation. To reduce such effects of condensation and coagulation on the measured J values, the measured N can be extrapolated at a specific D_p (e.g., 1 nm) (Kerminen and Kulmala, 2002; Kulmala et al., 2006). This normalization would

Laboratory studies of H_2SO_4/H_2O binay homogeneous nucleation

L.-H. Young et al.

allow one to obtain J values that are more representative of the "true" nucleation rates (i.e., the formation rate of the critical clusters). In the present study, we report the measured "apparent" formation rates to directly compare with other laboratory kinetics experiments.

4.4 Particle sizes (D_p) and growth rates

The sizes of the newly formed particles, D_p, were predominantly smaller than 10 nm (Figs. 8 and 11), indicating that nucleation takes place via the gas-phase homogeneous nucleation from the SO_2 + OH reaction (R1). In addition, the mode diameter of the newly formed particles shifts towards larger sizes with increasing N and [H_2SO_4]. For example, the mode diameter increased from 5.0 to 5.1, to 5.7 nm as t_n increased from 24 to 37, to 54 s (Fig. 9). This translates to growth rates roughly ranging from 28 to 127 nm h^{-1} (average ~84 nm h^{-1}). In field observations, on the other hand, the derived growth rates are in the range of 1 to 20 nm h^{-1} (Kulmala et al., 2004). The high particle growth rates taken from our experiments are probably due to the fact that the particle precursor concentrations were much higher than those in the atmosphere. But from the viewpoint of experimental design, however, large particle growth rates allow us to grow newly formed particles to measurable sizes (>2.5 nm) within a shorter timeframe (e.g., <60 s). To accommodate such high growth rates, very high initial [H_2SO_4] is required. On the other hand, the high initial [H_2SO_4] can also increase J and therefore, H_2SO_4 dependence of J can also be overestimated (Sect. 4.5.)

4.5 Dependence of nucleation rates (J) on [H_2SO_4], RH and nucleation time (t_n)

A summary of the measured [H_2SO_4] and J at 288 K, 97.3 kPa, and RH of 11%, 15%, and 23% is given in Table 3. At RH of 11%, the measured J ranged from 0.03 to 1.1 cm^{-3} s^{-1} for [H_2SO_4] (measured by CIMS at the end of the nucleation reactor) between 5.2×10^8 and 1.9×10^9 cm^{-3}. The estimated number of H_2SO_4 molecules (n) in the critical clusters ranged from 3 to 6. At RH of 15%, the measured J ranged from

0.02 to $8.5\,cm^{-3}\,s^{-1}$ for $[H_2SO_4]$ between 8.9×10^7 and $3.9\times10^9\,cm^{-3}$; the n values ranged from 4 to 8. At RH of 23%, the measured J ranged from 0.16 to $550\,cm^{-3}\,s^{-1}$ for $[H_2SO_4]$ between 8.7×10^7 and $9.6\times10^9\,cm^{-3}$; the n values were ~3. These n values were derived from the slopes of J vs. $[H_2SO_4]$ plots (Fig. 14).

5   Figure 14a shows the measured J as a function of $[H_2SO_4]$ from the present study from the SO_2 + OH reaction. We also included here the J values cited from earlier studies by Ball et al. (1999) and Berndt et al. (2006) for comparison (Fig. 14b). The data points from the present study fall between those from these two earlier studies. In this study, the slopes at RH of 23% are not as steep as that at RH of 11 and 15%; n
10 increased from ~3 to ~8 when RH decreased from 23% to 15%. These results indicate that there are less H_2SO_4 molecules in the critical clusters at higher RH, as predicted from the nucleation theories. The increased n with decreasing RH is consistent with nucleation theories and also consistent with Ball et al. (1999) and Berndt et al. (2005, 2006) results. The slopes at RH of 15%, however, are not distinctly different from that
15 at RH of 11% (4–8 vs. 3–6). Interestingly, the n values at RH of 15% and 10% from Ball et al. (1999) were also not very different from each other (7 vs. 8). Nevertheless, the n value increased from 7 to 13 when the RH was lowered from 15 to 2% in Ball et al. (1999). The data points from this study (group B) at RH of 15% and t_n of 19 s (from 100 ppm source cylinder experiments) nearly overlap with those from Ball et al. (1999)'s
20 liquid H_2SO_4 experiments at RH of 15%.

    In order to measure the H_2SO_4/H_2O binary J of $1\,cm^{-3}\,s^{-1}$, in the present study the minimum residual $[H_2SO_4]$ was at the $10^8\,cm^{-3}$ range at RH between 11 to 23% and 288 K (Fig. 14). In Berndt et al. (2005, 2006), however, the residual $[H_2SO_4]$ of ~$10^7\,cm^{-3}$ was sufficient to produce J of $1\,cm^{-3}\,s^{-1}$ at RH of 11%, 22%, and 288 K.
25 In Ball et al. (1999), $[H_2SO_4]$ of ~$10^9\,cm^{-3}$ was needed at RH between 2 and 15% and 295 K for binary and ternary (with NH_3) homogeneous nucleation. A recent re- fined kinetic quasi-unary nucleation model for H_2SO_4/H_2O shows that the initial (or nucleation-zone) $[H_2SO_4]$ has to be at least $10^{11}\,cm^{-3}$ to observe significant binary J at RH<20% and 300 K (Yu, 2007).

The number of H_2SO_4 molecules in the critical clusters obtained from laboratory studies of H_2SO_4/H_2O binary homogenous nucleation is typically larger than 3 and even up to ~30 for $[H_2SO_4]$ between ~10^7 to 10^{11} molecules cm^{-3} (this study; Wyslouzil et al., 1991; Viisanen et al., 1997; Ball et al., 1999; Berndt et al., 2005; Berndt et al., 2006; Benson et al., 2008). These numbers are much higher than those actually observed in the atmospheres. Field studies have shown that that the number of H_2SO_4 molecules in the critical clusters is often between one and two (Weber et al., 1996; Sihto et al., 2006; McMurry and Eisele, 2005). Such discrepancy raises questions on whether the binary homogeneous nucleation is the primary nucleation mechanism in the atmosphere. Recently, Kulmala et al. (2006) proposed an activation theory of ion or neutral clusters containing one or two H_2SO_4 molecules to explain the field observations, but further experimental work will be required to prove their theory.

4.6 H_2SO_4 and particle formation in the absence of OH

Although it is not the focus of the present study, we observed that H_2SO_4 and particle formation in the absence of OH, i.e., only from SO_2, O_2, and water vapor. There are several experimental results related to this observation. Firstly, this feature is shown in Fig. 4. Secondly, it was consistent from our experiments that the measured $[H_2SO_4]$ and particles were directly related to the initial $[SO_2]$ (Figs. 4–12), even though $[SO_2] \gg [OH]$ and therefore, the produced $[H_2SO_4]$ from (R1) should be the same as [OH] and independent from $[SO_2]$. Finally, the estimated growth rates (28 to 127 nm h^{-1}) from our experiments are much higher than those predicted from the initial $[H_2SO_4]$ of 10^9 cm^{-3} (Fig. 2b). These results suggest that there may be some unknown oxidation processes in the absence of OH, related to H_2SO_4 and new particle formation. However, future studies are required to better understand the mechanisms involved in these processes.

5 Conclusions

We have developed a laboratory experimental set up to study the binary homogeneous nucleation H_2SO_4/H_2O. This setup design is largely based on Ball et al. (1999) and Berndt et al. (2005). Specifically, our nucleation reactor has similar dimension and flow rates as in Ball et al. (1999) and both these two studies directly measure $[H_2SO_4]$ with CIMS at the end of the nucleation reactor. We also produce H_2SO_4 vapor at in-situ from the $SO_2 + OH \rightarrow HSO_3$ reaction similarly to Berndt et al. (2005, 2006). However, unlike Berndt et al. (2005, 2006), OH is produced from the water UV absorption, which also allows for direct measurements of [OH] with accurate photon flux measurements and thus the initial $[H_2SO_4]$. In the present study, we provide a systematic evaluation of this new nucleation experimental system from various technical aspects and discuss our primarily BHN results by comparing with other laboratory studies.

Binary homogeneous nucleation rates of H_2SO_4/H_2O were measured using $SO_2 + OH \rightarrow HSO_3$ at 288 K, 97.3 kPa, RH from 6 to 23% for the H_2SO_4 residual concentrations from 10^8 to 10^{10} cm^{-3} and t_n between 5 and 59 s. Wall loss factors of H_2SO_4 are also provided as a function of nucleation time and diameter of the nucleation reactor. The measured nucleation rates ranged from 0.02 and 550 cm^{-3} s^{-1} and increased with increasing $[H_2SO_4]$ and RH. Such trends are consistent with the predictions of nucleation theories. Under our experimental conditions, at least 10^8 cm^{-3} of H_2SO_4 molecules were needed to produce the nucleation rate of 1 cm^{-3} s^{-1}. This $[H_2SO_4]$ threshold falls between 10^7 cm^{-3} in Berndt et al. (2005, 2006) and 10^9 cm^{-3} in Ball et al. (1999), two earlier laboratory nucleation studies. The nucleation times used in our study are longer than that of Ball et al. (1999) (4 s), but shorter than that of Berndt et al. (2005, 2006) (560 and 290 s, respectively). These differences, together with different methods to produce and detect H_2SO_4, make a comparison of H_2SO_4 threshold for nucleation amongst different studies less straightforward, because different nucleation times and different dimensions of the nucleation reactor lead to different wall losses, particle sizes, and particle growth rates under similar precursor concentra-

tions.

The power relationship between measured nucleation rate and H_2SO_4 concentration suggests there are 3 to 8 H_2SO_4 molecules in the critical clusters under our experimental conditions. This number also increased with decreasing RH, in an agreement with classical nucleation theories, and is in the same range as those reported from the previous laboratory nucleation studies (Wyslouzil et al., 1991; Ball et al., 1999; Berndt et al., 2005; Berndt et al., 2006). The estimated numbers of H_2SO_4 molecules in the critical clusters from these laboratory studies are, however, much larger than those (between 1 and 2) derived from field observations (Weber et al., 1996; Sihto et al., 2006; McMurry and Eisele, 2005).

The measured sizes of newly-formed particles were smaller than 10 nm and the derived growth rates ranged from 28 to 127 nm h^{-1}. Both particle sizes and concentrations increased with increasing t_n, [H_2SO_4], and RH. These trends are also consistent with nucleation theories (Kulmala et al., 2004). However, these results also indicate that the particle number concentrations, which are used for nucleation rate calculation, are not necessarily on the same basis, size-wise, when comparing the results from different studies and even different experiments within the same laboratory studies.

While these experimental results demonstrate a strong validation of our nucleation kinetics setup and also provide important nucleation properties which are in fact consistent with predictions from the nucleation theories, there are also several difficulties that are inherited in the laboratory experiments of H_2SO_4/H_2O nucleation studies. The CIMS-measured H_2SO_4 concentrations are not the initial concentrations, but rather the residual or equilibrium concentrations, because a large fraction of the initially formed H_2SO_4 molecules are lost to the flow reactor wall and by condensation growth. In addition, relatively high [H_2SO_4] was used in order to form particles at measurable sizes (>3 nm) within the short nucleation time (<60 s). High wall losses of H_2SO_4 are also responsible for high [H_2SO_4] used in the present study due to large surface-to-volume ratio of our nucleation reactor. Under high [H_2SO_4] and number concentrations, condensation and coagulation also begin to compete with nucleation, which in turn may

Laboratory studies of H_2SO_4/H_2O binay homogeneous nucleation

L.-H. Young et al.

also affect the H_2SO_4 dependence of nucleation rates. Nucleation time is another important technical aspect for nucleation experiments. With increasing nucleation times, the number concentrations and sizes of newly-formed particles increased, whereas the residual $[H_2SO_4]$ decreased. The former implies the nucleation is still active within the

5 nucleation time frame of the present experimental setup, and the latter shows that the measured $[H_2SO_4]$ could be underestimated because of the H_2SO_4 wall losses and condensation growth.

Our future goal is to measure nucleation rates at atmospherically relevant conditions with $[H_2SO_4]$ in the 10^6–10^7 cm^{-3} range with and without ternary species and compare

10 them with atmospherically observed nucleation rates. Thus far, our experiments shown here were made at higher $[H_2SO_4]$ ranging from 10^8–10^{10} cm^{-3}. Nevertheless, our nucleation experiments provide important kinetics properties of H_2SO_4/H_2O nucleation required to test nucleation theories and complement previous laboratory studies. We plan to quantitatively characterize the H_2SO_4 wall loss by simultaneously measuring

15 H_2SO_4 at the beginning and end of the nucleation reactor and provide more accurate information on particle precursor concentrations for future nucleation experiments.

References

Ball, S. M., Hanson, D. R., Eisele, F. L., and McMurry, P. H.: Laboratory studies of particle nucleation: Initial results for H_2SO_4, H_2O, and NH_3 vapors, J. Geophys. Res., 104, 23 709–23 718, 1999.
25 Baron, P. A. and Willeke, K. (eds.): Aerosol measurement: principles, techniques, and applications, 2nd ed., John Wiley and Sons, New York, 2001.
Benson, D. R., Young, L. H., Kameel, F. R., and Lee, S. H.: Laboratory-measured nucleation

rates of sulfuric acid and water binary homogeneous nucleation from the SO_2 + OH reaction, Geophys. Res. Lett., in press, doi:10.1029/2008GL033387, 2008

Berndt, T., Böge, O., Stratmann, F., Heintzenberg, J., and Kulmala, M., Rapid formation of sulphuric acid particles at near-atmospheric conditions, Science, 307, 698–700, 2005.

Berndt, T., Böge, O., and Stratmann, F.: Formation of atmospheric H_2SO_4/H_2O particles in the absence of organics: a laboratory study, Geophys. Res. Lett., 33, L15817, doi:10.1029/2006GL026660, 2006.

Berndt, T., Böge, O., and Stratmann, F.: Atmospheric H_2SO_4/H_2O particle formation: Mechanistic Investigation, Proceeding for the 17th International Conference on Nucleation and Atmospheric Aerosols., Galway, Ireland, editd by: O'Dowd, C. D. and Wagner, P., pages 69–72, Springer, 2007.

Boulaud, D., Madelaine, G., Vigla, D., and Bricard, J.: Experimental study on the nucleation of water vapor sulphuric acid binary system, J. Chem. Phys., 66, 4854–4860, 1977.

Cantrell, C. A., Zimmer, A., and Tyndall, G. S.: Absorption cross sections for water vapor from 183 to 193 nm, Geophys. Res. Lett., 24, 2195–2198, 1997.

Christensen, P. S., Wedel, S., and Livbjerg, H.: The kinetics of the photolytic production of particles from SO_2 and NH_3 in humid air, Chem. Eng. Sci., 49, 4605–4614, 1994.

DeMore, W. B., Sander, S. P., Golden, D. M., Hampson, R. F., Kurylo, M. J., Howard, C. J., Ravishankara, A. R., Kolb, C. E., and Molina, M. J.: Chemical kinetics and photochemical data for use in stratospheric modeling, Evaluation number 12, JPL Publ. 97-4, NASA Jet Porpulsion Lab., Pasadena, CA, 1997.

Diamond, G. L., Iribarne, J. V., and Corr, D. J.: Ion-induced nucleation from sulphur dioxide, J. Particle Sci., 16, 43–55, 1985.

Eisele, F. L. and Tanner, D. J.: Measurement of the gas-phase concentration of H2SO4 and methane sulphonic-acid and estimates of H_2SO_4 production and loss in the atmosphere, J. Geophys. Res., 98, 9001–9010, 1993.

Hanson, D. R. and Eisele, F.: Diffusion of H_2SO_4 in humidified nitrogen: Hydrated H_2SO_4, J. Phys. Chem. A, 104, 1715–1719, 2000.

Huey, L. G.: Measurement of trace atmospheric species by chemical ionization mass spectrometry: Speciation of reactive nitrogen and future directions, Mass Spectrom. Rev., 26, 166–184, 2007.

Kashchiev, D.: On the relation between nucleation work, nucleus size and nucleation rate, J. Chem. Phys., 76, 5098–5102, 1982.

Laboratory studies of H_2SO_4/H_2O binay homogeneous nucleation

L.-H. Young et al.

Kerminen, V.-M. and Kulmala, M.: Analytical formulae connecting the "real" and the "apparent" nucleation rate and the nuclei number concentration for atmospheric nucleation events, J. Aerosol Sci., 33, 609–622, 2002.

Kim, T. O., Adachi, M., Okuyama, K., and Seinfeld, J. H.: Experimental measurement of competitive ion-induced and binary homogeneous nucleation in $SO_2/H_2O/N_2$ mixtures, Particle Sci. Technol., 26, 527–543, 1997.

Korhonen, P., Kulmala, M., Laaksonen, A., Viisanen, Y., McGraw, R., and Seinfeld, J. H.: Ternary nucleation of H_2SO_4, NH_3, and H_2O in the atmosphere, J. Geophys. Res., 104, 26 349-26 353, 1999.

Kulmala, M., Vehkamäki, H., Petäjä, T., Dal Maso, M., Lauri, A., Kerminen, V.-M., Birmili, W., and McMurry, P. H.: Formation and growth rates of ultrafine atmospheric particles: a review of observations, J. Aerosol Particle Sci., 35, 143–176, 2004.

Kulmala, M., Lehtinen, K. E. J., and Laaksonen, A.: Cluster activation theory as an explanation of the linear dependence between formation rate of 3 nm particles and sulphuric acid concentration, Atmos. Chem. Phy., 6, 787–793, 2006.

Lee, S.-H., Reeves, J. M., Wilson, J. C., Hunton, D. E., Viggiano, A. A., Miller, T. M., Ballenthin, J. O., and Lait, L. R.: Particle formation by ion nucleation in the upper troposphere and lower stratosphere, Science, 301, 1886–1889, 2003.

Lovejoy, E. R., Curtius, J., and Froyd, K. D.: Atmospheric ion-induced nucleation of sulphuric acid and water, J. Geophys. Res., 109, D08204, doi:10.1029/2003JD004460, 2003.

Mäkelä, J. M., Jokinen, V., and Kulmala, M.: Small ion mobilities during particle formation from irradiated SO_2 in humid air, J. Particle Sci., 26, Sppl. 1, S333–S334, 1995.

McMurry, P. H. and Eisele, F. L.: Preface to topical collection on new particle formation in Atlanta, J. Geophys. Res., 110, D22S01, doi:10.1029/2005JD006644, 2005.

Mirabel, P. and Clavelin, J. L.: Experimental study of nucleation in binary mixtures: The nitric acid-water and sulphuric acid-water systems, J. Chem. Phys., 68, 5020–5027, 1978.

Napari, I., Noppel, M., Vehkamäki, H., and Kulmala, M.: Parameterization of ternary nucleation rates for H_2SO_4-NH_3-H_2O vapors, J. Geophys. Res., 107(D19), 4381, doi:10.1029/2002JD002132, 2002.

National Institute for Standard Technology (NIST) Chemistry Web Book, NIST Standard Reference Database Number 69, June 2005 Release, available at: http://webbook.nist.gov/chemistry/, 2005.

Reiss, H., Margolese, D. I., and Schelling, F. J.: Experimental study of nucleation in vapor

Laboratory studies of H_2SO_4/H_2O binay homogeneous nucleation

L.-H. Young et al.

mixtures of sulphuric acid and water, J. Colloid Interf. Sci., 56, 511–526, 1976.

Seinfeld, J. H. and Pandis, S. N.: Atmospheric chemistry and physics: from air pollution to climate change, Wiley, New York, 1998.

Sihto S.-L., Kulmala, M., Kerminen, V.-M., Dal Maso, M., Petäjä, T., Riipinen, L., Korhonen, H., Arnold, F., Jason, R., Boy, M., Laaksonen, A., and Lehtinen, K. E. J.: Atmospheric sulphuric acid and aerosolparticle formation: implications from atmospheric measurements for nucleation and early growth mechanisms, Atmos. Chem. Phys., 6, 4079–4091, 2006, http://www.atmos-chem-phys.net/6/4079/2006/.

Strey, R. and Viisanen, Y.: Measurement of the molecular content of binary nuclei: use of the nucleation rate surface for ethanol-hexanol, J. Chem. Phys., 99, 4693–4704, 1993.

Vehkamäki, H., Kulmala, M., Napari, I., Lehtinen, K. E. J., Timmreck, C., Noppel, M., and Laaksonen, A.: An improved parameterization for sulphuric acid-water nucleation rates for tropospheric and stratospheric conditions, J. Geophys. Res., 107, 4622, doi:10.1029/2002JD002184, 2002.

Viggiano, A. A., Seeley, J. V., Mundis, P. L., Williamson, J. S., and Morris, R. A.: Rate constants for the reactions of $XO_3^-(H_2O)_n$ (X=C, HC, and N) and $NO_3^-(HNO_3)_n$ with H_2SO_4: implications for atmospheric detection of H_2SO_4, J Phys. Chem. A, 101, 8275–8278, 1997.

Viisanen, Y., Kulmala, M., and Laaksonen, A.: Experiments on gas-liquid nucleation of sulphuric acid and water, J. Chem. Phys., 107, 920–926, 1997.

Weber, R. J., Marti, J. J., McMurry, P. H., Eisele, F. L., Tanner, D. J., and Jefferson, A.: Measured atmospheric new particle formation rates: implications for nucleation mechanisms, Chem. Eng. Commun., 151, 53–64, 1996.

Wyslouzil, B. E., Seinfeld, J. H., Flagan, R. C., and Okuyama, K.: Binary nucleation in acid-water systems. II. Sulphuric acid-water and a comparison with methanesulphonic acid-water, J. Chem. Phys., 94, 6842–6850, 1991.

Yu, F.: Improved quasi-unary nucleation model for binary H_2SO_4–H_2O homogenous nucleation, J. Chem. Phys., 127, 054301-1–054301-8, 2007.

Yu, F., and Turco, R. P.: Ultrafine aerosol formation via ion-mediated nucleation, Geophys. Res. Lett., 27, 883–886, 2000.

Zhang, R., Suh, I., Zhao, J., Zhang, D., Fortner, E. C., Tie, X., Monila, L. T., and Monila, M. J.: Atmospheric new particle formation enhanced by organic acids, Science, 304, 1487–1490, 2004.

Laboratory studies of H$_2$SO$_4$/H$_2$O binay homogeneous nucleation

L.-H. Young et al.

ACPD

8, 6903–6947, 2008

Laboratory studies of H$_2$SO$_4$/H$_2$O binay homogeneous nucleation

L.-H. Young et al.

Title Page	
Abstract	Introduction
Conclusions	References
Tables	Figures

◄◄	►►

◄	►

Back	Close

Full Screen / Esc

Printer-friendly Version

Interactive Discussion

Table 1. A summary of the previous laboratory studies of H$_2$SO$_4$–H$_2$O BHN, along with two studies from our group. $n_{H_2SO_4}$ indicates the number of H$_2$SO$_4$ in the critical clusters, n_{H_2O} the number of H$_2$O molecules in the critical clusters, CIMS chemical ionization mass spectrometry, and (R1) the SO$_2$ + OH → HSO$_3$ reaction. [H$_2$SO$_4$] are the residual [H$_2$SO$_4$] measured by CIMS at the end of the nucleation reactor.

Reference	H$_2$SO$_4$ Production	Measurement of H$_2$SO$_4$	[H$_2$SO$_4$] (cm^{-3})	RH (%)	J (cm^{-3} s^{-1})	$n_{H_2SO_4}$; n_{H_2O}
Wyslouzil et al., 1991	Liquid H$_2$SO$_4$	Mass balance calculation	1.3×10^{10} to 1.5×10^{11}	0.6 to 65	0.001 to 300	4 to 30; 9
Viisanen et al., 1997	Liquid H$_2$SO$_4$	Mass balance calculation	1×10^{10} to 3×10^{10}	38 and 52	2 to 3000	21 and 10; –
Ball et al., 1999	Liquid H$_2$SO$_4$	CIMS	2.5×10^9 to 1.2×10^{10}	2 to 15	0.01 to 1000	7 to 13; 4 to 6
Zhang et al., 2004	Liquid H$_2$SO$_4$	CIMS	4×10^9 to 1×10^{10}	5	0.3 to 500	
Berndt et al., 2005, 2006	(R1)	Organic titration reactions and kinetic model calculation	1×10^7 to 1×10^8	11 to 60	0.1 to 100,000	4 to 6; –
Benson et al., 2008	(R1)	CIMS	3×10^6 to 2×10^9	11 to 50	0.1 to 10,000	2 to 10; 10 to 15
This study	(R1)	CIMS	1×10^8 to 1×10^{10}	6 to 23	0.02 to 550	3 to 8; –

Laboratory studies of H$_2$SO$_4$/H$_2$O binay homogeneous nucleation

L.-H. Young et al.

Table 2. Experimental conditions used in the present study (288 K and 97.3 kPa).

| SO$_2$ Source | Flow Reactor | | Total Flow | SO$_2$ Flow | RH (%) | Nucleation Time |
	ID (cm)	Length (cm)	(lpm)	(lpm)		(s)
2.5 ppm ^{34}SO$_2$	2.54	80	2.5 to 4.8	0.15 to 2.0	6 to 15	5 to 10
1 ppm ^{32}SO$_2$	2.54	80	2.5	0.1 to 0.9	12 to 17	10
1 ppm ^{32}SO$_2$	5.08	82	1.7 to 5.3	0.1 to 0.9	13 to 15	19 to 59
100 ppm ^{32}SO$_2$	5.08	82	1.7 to 5.3	0.001 to 0.2	9 to 23	19 to 59

Table 3. A summary of the measured residual [H$_2$SO$_4$] and J for SO$_2$ with OH experiments at RH of 11, 15, and 23% (288 K and 97.3 kPa) (corresponding to Fig. 14a). n is the number of H$_2$SO$_4$ molecules in the critical clusters.

RH (%)	No. of Data	[H$_2$SO$_4$] (cm^{-3})		J (cm^{-3} s^{-1})		n
		Min	Max	Min	Max	
11	29	5.2×10^8	1.3×10^9	0.03	1.1	3–6
15	136	8.9×10^7	3.9×10^9	0.02	8.5	4–8
23	54	8.7×10^7	9.6×10^9	0.16	550	~3
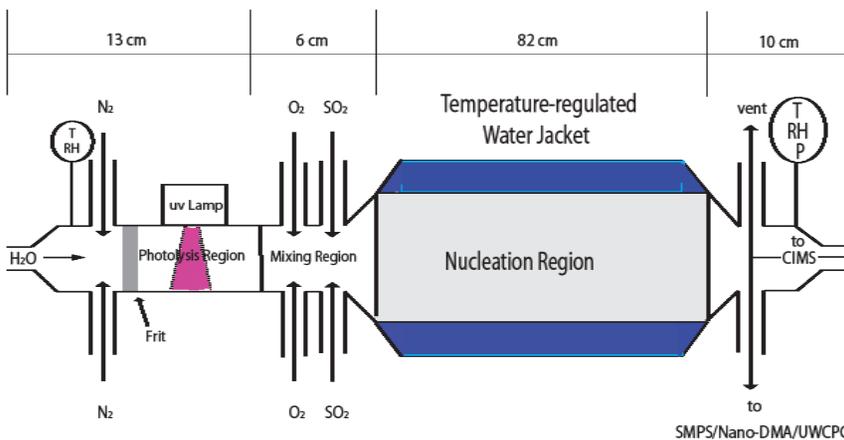
Fig. 1. A schematic diagram of the Kent State University Sulphuric Acid-Water BHN experimental setup.
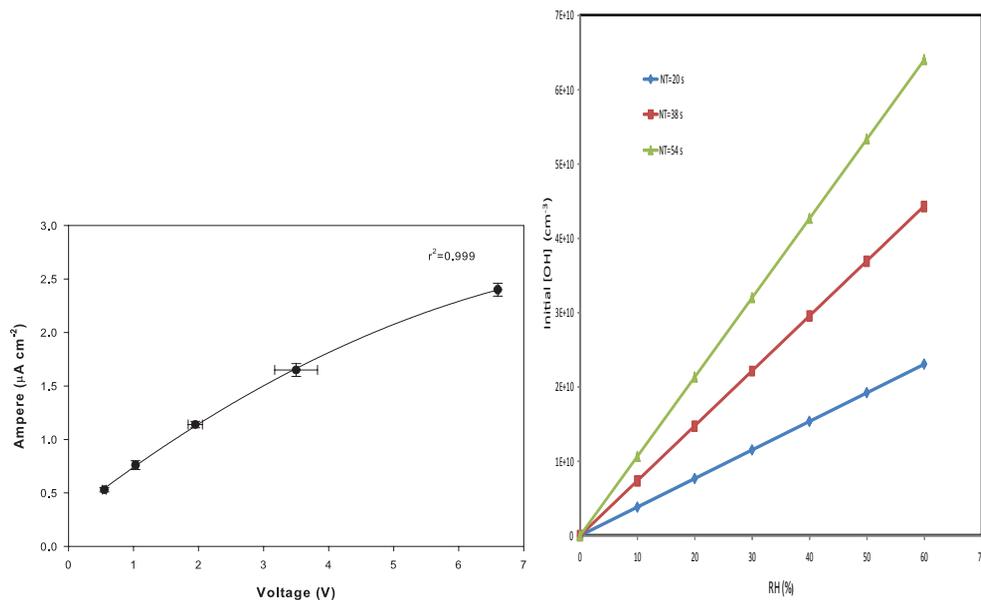
Fig. 2. The calculated [OH] produced from water UV absorption as a function of RH and nucleation time (t_n) (see Sect. 2.1 for the detail). Different nucleation times imply different total flows used and hence, different photolysis times (t_p). For example, under the present experimental conditions, for t_n=20 s, t_p=0.08 s; for t_n=38 s, t_p=0.15 s; for t_n=54 s, t_p=0.21 s. Since at the typical experimental conditions [SO$_2$]≫[OH], the produced initial [H$_2$SO$_4$]=[OH].
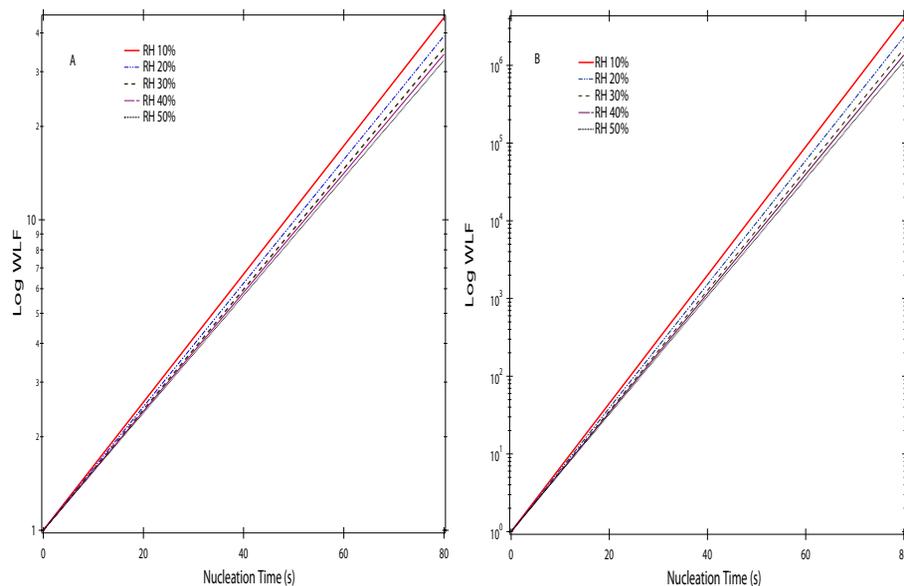
Fig. 3. The calculated wall loss factors (WLFs) as a function of nucleation time and RH for the nucleation reactor with I.D. of **(a)** 5.08 cm and **(b)** 2.54 cm. In this calculation, we assumed that wall loss is a diffusion limited process based on Hanson and Eisele (2000), as described in Benson et al. (2008).

(a) Run sequence

(2) +SO$_2$

(3) OH

(4)

-SO$_2$

Sulfuric acid signal

+O$_2$/H$_2$O

+OH

(1)

Time

(b) RH = 15 %, t_n = 19 s

[SO$_2$] = 0.12 ppm   0.09 ppm   0.08 ppm

H$_2$SO$_4$
Particle number

[H$_2$SO$_4$] (cm^{-3})

Particle Number (cm^{-3})

11:00 AM   11:15 AM   11:30 AM   11:45 AM
Local Time
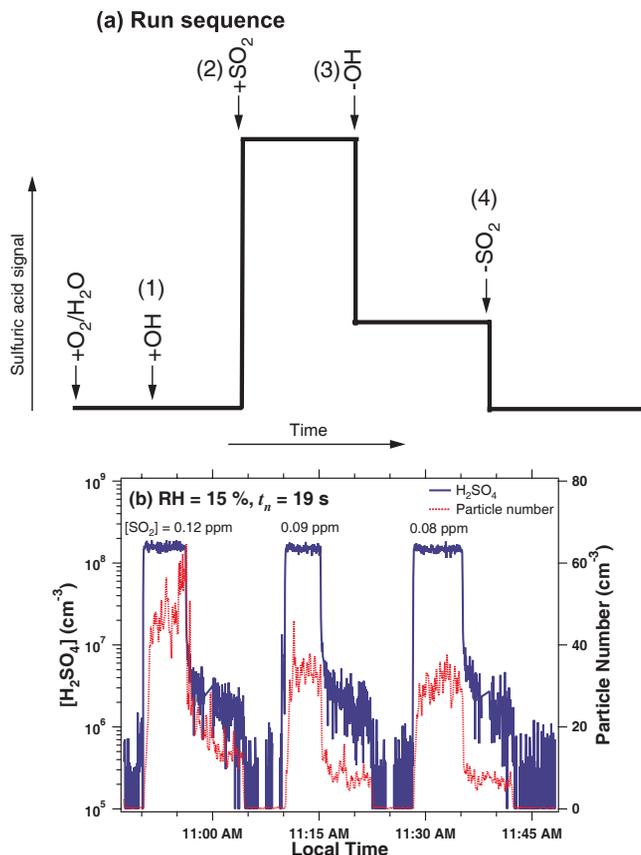
Fig. 4. Experimental procedure and results to investigate the effects of SO$_2$ and OH on the production of H$_2$SO$_4$ and particles at 288 K. **(a)** The experimental run sequence. **(b)** The CIMS-measured residual [H$_2$SO$_4$] and particle number concentration in response to running the sequence three times of varying SO$_2$ concentration. Note the residual [H$_2$SO$_4$] is in log scale.
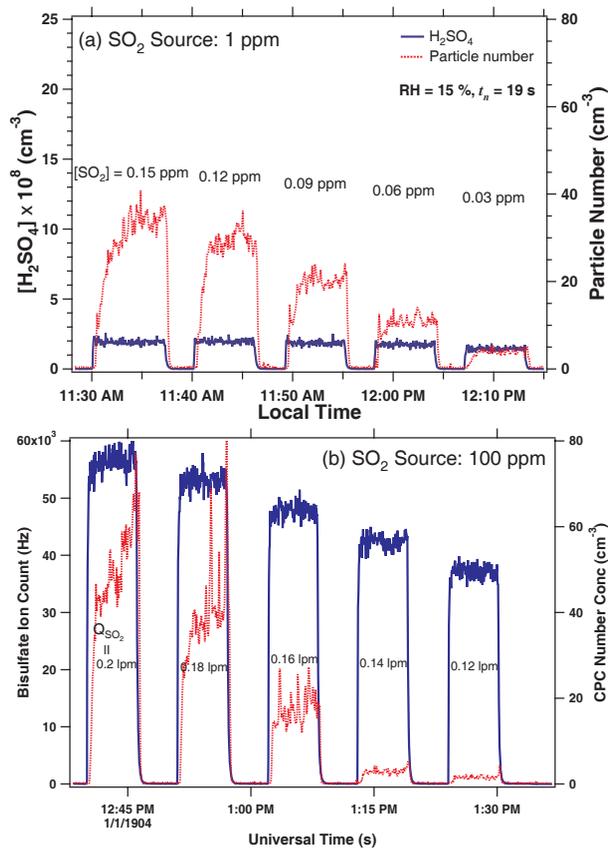
Fig. 5. The measured particle number concentrations as a function of the residual [H$_2$SO$_4$] with the 1 ppm **(a)** and 100 ppm **(b)** SO$_2$ source cylinder at 288 K. The initial [SO$_2$] are shown in ppm in the figures.

ACPD

8, 6903–6947, 2008

Laboratory studies of H₂SO₄/H₂O binay homogeneous nucleation

L.-H. Young et al.

Title Page

Abstract   Introduction

Conclusions   References

Tables   Figures

◄   ►

Back   Close

Full Screen / Esc

Printer-friendly Version

Interactive Discussion
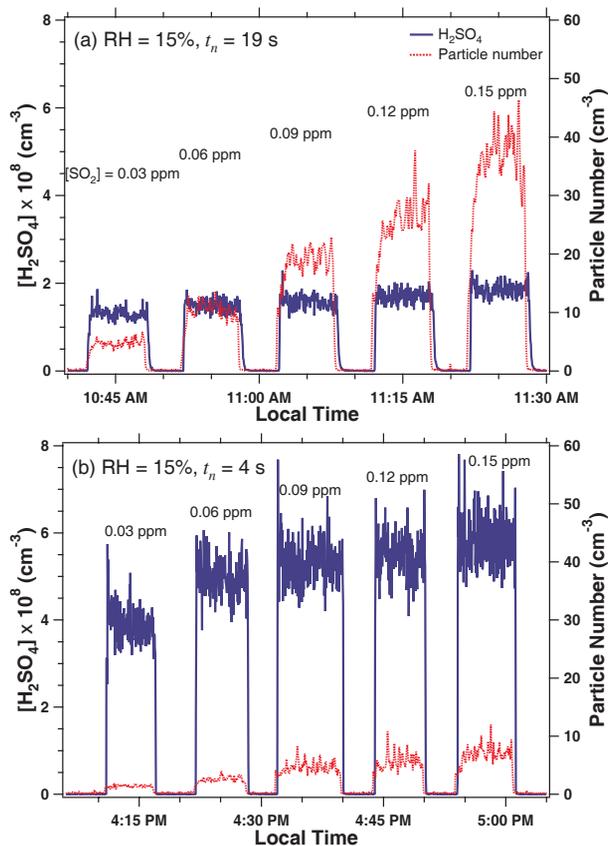
Fig. 6. The measured particle number concentrations as a function of the residual [H$_2$SO$_4$] with **(a)** nucleation time t_n=19 s and **(b)** t_n=4 s at 288 K. The initial [SO$_2$] are shown in ppm in the figures.
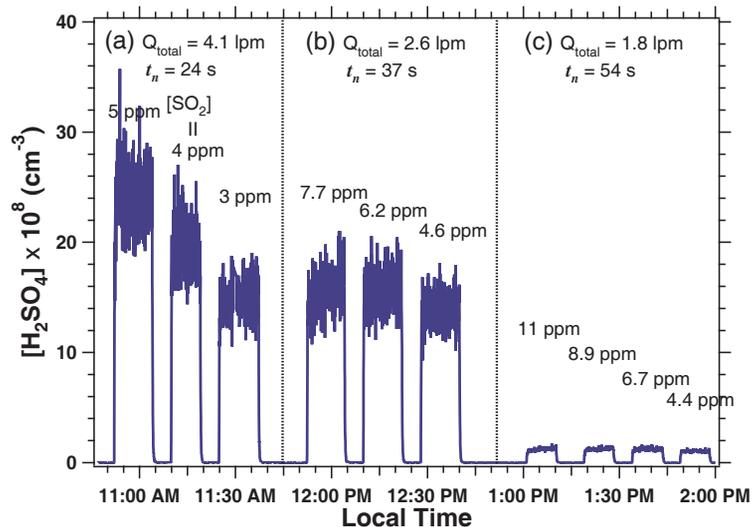
Fig. 7. The CIMS-measured residual [H$_2$SO$_4$] at varying total flow rate Q_{total} and nucleation time t_n at RH of 23% and 288 K. The measured number size distributions of these particles are shown in Fig. 8.
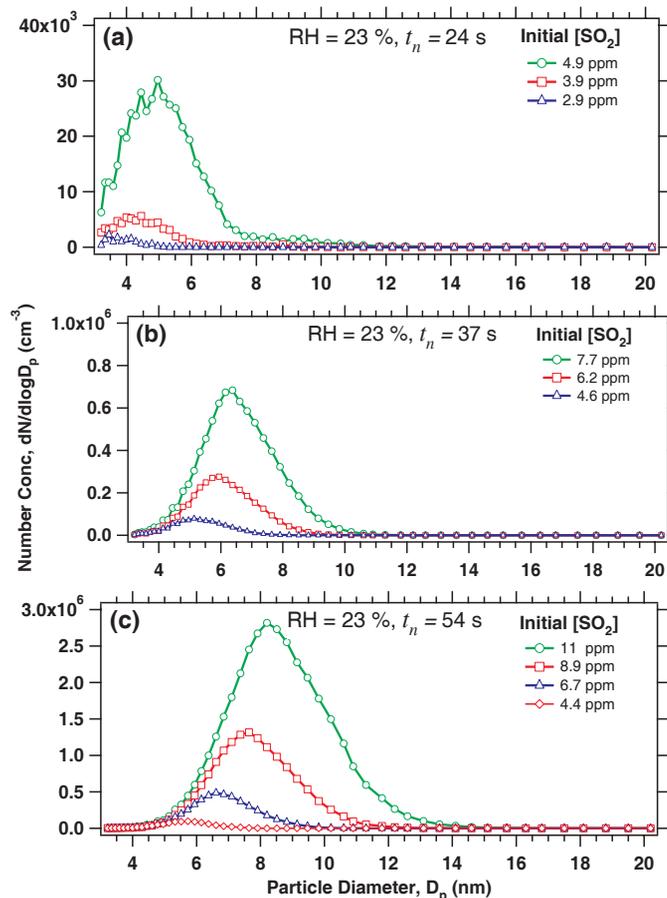
Fig. 8. The average number size distributions of newly formed particles at varying total flow rates Q_{total}, initial SO$_2$ concentrations, and nucleation times t_n at 288 K. These datasets are same as those used in Fig. 7. Note the scales of the y axes are different.
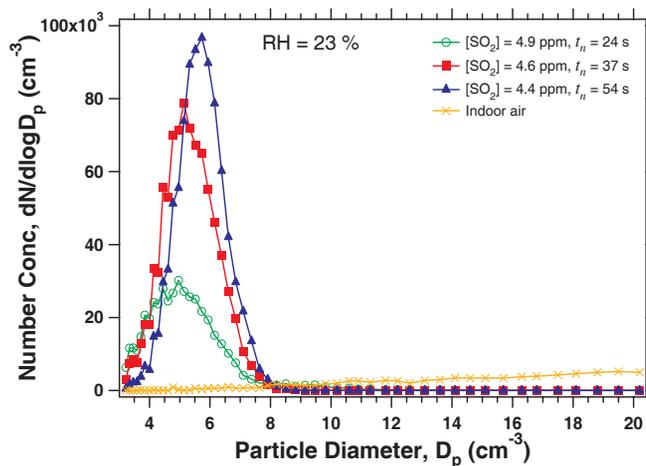
Fig. 9. The average number size distributions measured at similar initial SO$_2$ concentrations but varying nucleation time t_n at 288 K. These datasets are also used in Figs. 7 and 8.
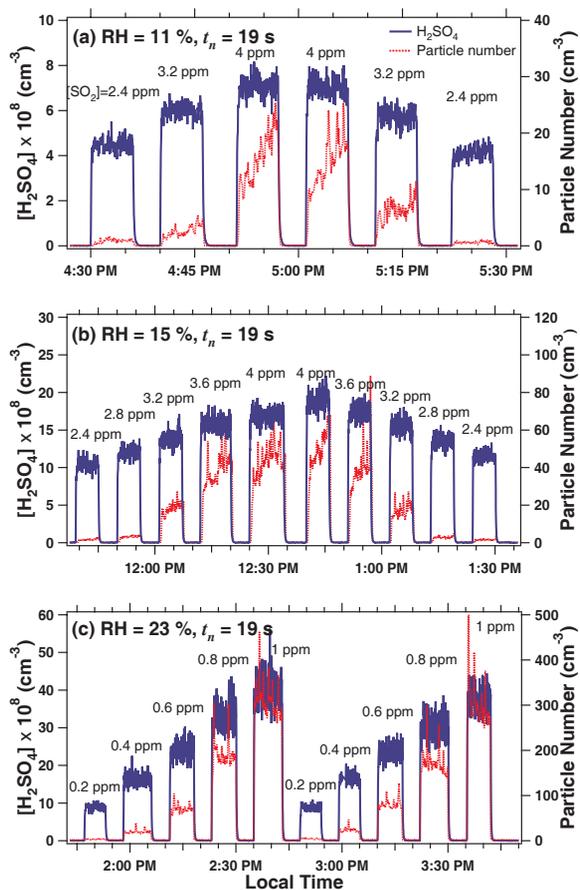
Fig. 10. The measured particle number concentrations as a function of the residual [H_2SO_4] at **(a)** RH=11%, **(b)** RH=15%, and **(c)** RH=23% at 288 K. Note the scales of the y axes are different. The initial [SO_2] are shown in ppm in the figures.
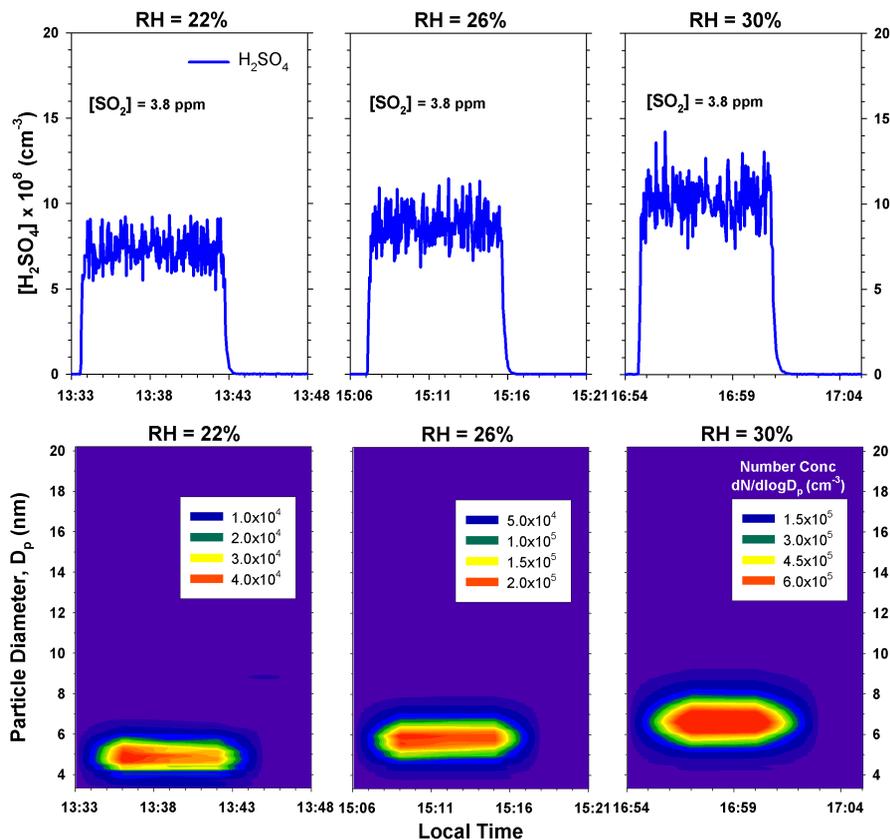
Fig. 11. The CIMS-measured residual H_2SO_4 and number size distributions of newly formed particles at **(a)** RH=22% (left panels), **(b)** RH=26% (middle panels), and **(c)** RH=30% (right panels) at 288 K. Note the scales for the number concentration are different. The initial [SO_2] are shown in ppm in the figures.

Printer-friendly Version

Interactive Discussion
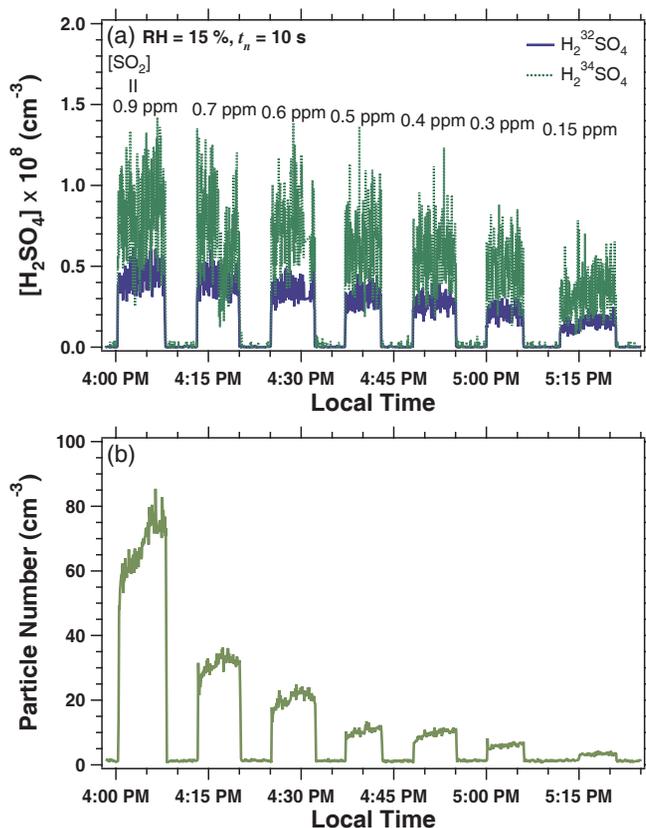
Fig. 12. The measured particle number concentration as a function of the residual $[H_2SO_4]$ from $^{34}SO_2$ + OH experiments at 288 K.

SO$_2$+OH+O$_2$+H$_2$O ┈┈▶ H$_2$SO$_4$

Flow direction

(a) (b) (c)
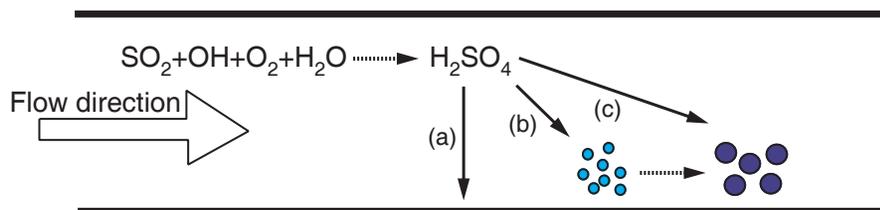
Fig. 13. Hypothetical loss processes that take place during the formation of H$_2$SO$_4$ from the SO$_2$ + OH → HSO$_3$ reaction in the flow reactor and the subsequent particle nucleation. Solid arrows indicate three pathways related to gas phase H$_2$SO$_4$ losses, **(a)** wall loss, **(b)** nucleation, and **(c)** condensation on the formed particles. The simulations of the time variation of OH and H$_2$SO$_4$ concentrations in the gas phase and H$_2$SO$_4$ concentrations in the aerosol phase and on the wall due to wall loss as a function of reaction time are shown by Benson et al. (2008).
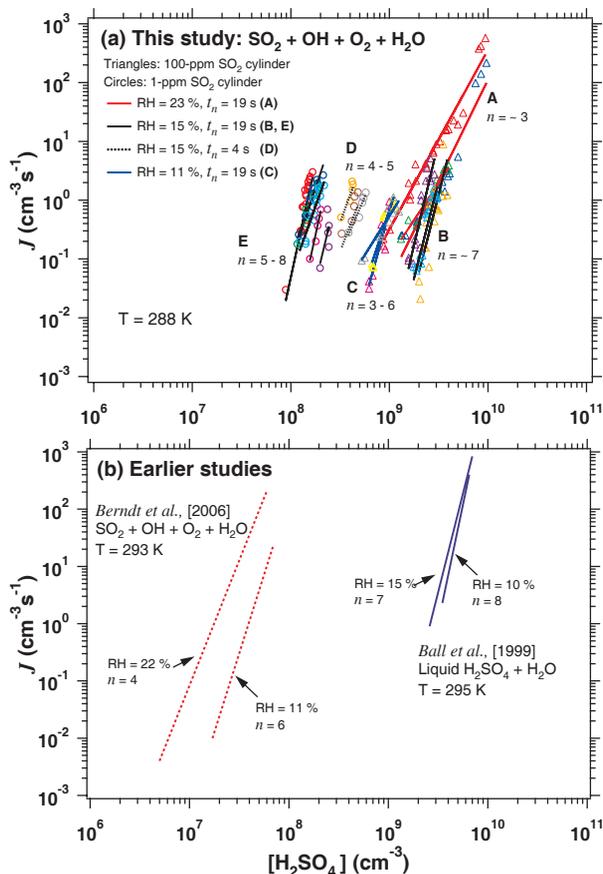
Fig. 14. The measured nucleation rates J as a function of $[H_2SO_4]$ for **(a)** the present SO_2 + OH experiments and **(b)** from earlier studies. The linear lines are the results of power regression on the experimental data. The calculated wall loss factors (WLFs) corresponding to our experimental conditions are shown in Fig. 3. In Ball et al. (1999), WLF=22. Berndt et al. (2006) did not provide WLFs.